Arctic Ocean gravity field derived from ICESat and ERS-2 altimetry: Tectonic implications

David C. McAdoo,[1] Sinead Louise Farrell,[1,2] Seymour W. Laxon,[2] H. Jay Zwally,[3] Donghui Yi,[4] and Andy L. Ridout[2]

Received 8 June 2007; revised 10 August 2007; accepted 18 January 2009; published 23 May 2008.

[1] A new, detailed marine gravity field for the persistently ice-covered Arctic Ocean, derived entirely from satellite data, reveals important new tectonic features in both the Amerasian and Eurasian basins. Reprocessed Geoscience Laser Altimeter System (GLAS) data collected by NASA's Ice Cloud and land Elevation Satellite (ICESat) between 2003 and 2005 have been combined with 8 years worth of retracked radar altimeter data from ESA's ERS-2 satellite to produce the highest available resolution gravity mapping of the entire Arctic Ocean complete to 86°N. This ARCtic Satellite-only (ARCS) marine gravity field uniformly and confidently resolves marine gravity to wavelengths as short as 35 km. ARCS relies on a Gravity Recovery and Climate Experiment (GRACE)-only satellite gravity model at long (>580 km) wavelengths and plainly shows tectonic fabric and numerous details imprinted in the Arctic seafloor, in particular, in the enigmatic Amerasian Basin (AB). For example, in the Makarov Basin portion of the AB, two north-south trending lineations are likely clues to the highly uncertain seafloor spreading history which formed the AB.

Citation: McAdoo, D. C., S. L. Farrell, S. W. Laxon, H. J. Zwally, D. Yi, and A. L. Ridout (2008), Arctic Ocean gravity field derived from ICESat and ERS-2 altimetry: Tectonic implications, *J. Geophys. Res.*, *113*, B05408, doi:10.1029/2007JB005217.

1. Introduction

1.1. Tectonic Background: Arctic Ocean Basin

[2] The origin and tectonic history of the world's major ocean basins are generally well known. However, the Arctic Basin is the notable exception. The Arctic Basin is composed of two parts: the relatively young (Cenozoic) Eurasian Basin (EB) which lies to one side (below and to the right in Figure 1) of the Lomonosov Ridge (LR) and the older, larger Amerasian Basin (AB) which lies on the other side of the LR (Figure 1). The EB has a fairly well understood origin: it has developed via slow seafloor spreading along the Gakkel Ridge [*Cochran et al.*, 2003; *Ostenso and Wold*, 1973] which commenced in the early Cenozoic (~55 Ma BP) and which remains active at present. However, the Amerasian Basin (AB) is the focus of the large tectonic uncertainty associated with the Arctic Ocean. The AB has been described [*Tessensohn and Roland*, 2000, p. 1] as an "enigmatic rounded deep hole surrounded by continents and without a clearly detectable mid-ocean ridge." The AB is thought to be tectonically inactive at present and to have formed in the late Mesozoic (Neocomian; ~130 Ma) [*Grantz et al.*, 1990, 1998; *Taylor et al.*, 1981; *Cochran et al.*, 2006], but this is also uncertain. A broad range of loosely constrained, substantially differing tectonic models of the AB's origin and development have been proposed. This range of tectonic models, specifically those dealing with the Canada basin portion of the overall AB, was outlined by *Lawver and Scotese* [1990] and debate continues today as to which of these widely differing models is correct. Moreover this uncertain tectonic history of the AB limits our ability to construct precise paleoclimate and paleo-oceanographic models of the Arctic.

1.2. Recent Arctic Ocean Gravity and Bathymetry

[3] The large uncertainty surrounding the origin of the AB owes in part to persistent sea ice which limits access by surface research vessels and in part to thick layers of sediments which mask any fossil mid-ocean ridge system in the AB. However, in the past 13 years, large amounts of Arctic gravity and bathymetry data have been either newly collected, or declassified and released. Some notable examples include the International Bathymetric Chart of the Arctic Ocean (IBCAO) (see Figure 1 and *Jakobsson et al.* [2000]), as well as a gravity compilation and model, the Arctic Gravity Project (ArcGP) [*Forsberg and Kenyon*, 2004; http://earth-info.nga.mil/GandG/wgs84/agp/readme_new.html]. ArcGP was developed by an international working group by combining available surface (mostly), airborne and submarine gravity data. Also between 1993 and 1999

[1]NOAA Laboratory for Satellite Altimetry, Silver Spring, Maryland, USA.
[2]Centre for Polar Observation and Modelling, University College London, London, UK.
[3]Cryospheric Sciences Branch, NASA Goddard Space Flight Center, Greenbelt, Maryland, USA.
[4]SGT, Inc., NASA Goddard Space Flight Center, Greenbelt, Maryland, USA.

Copyright 2008 by the American Geophysical Union.
0148-0227/08/2007JB005217$09.00

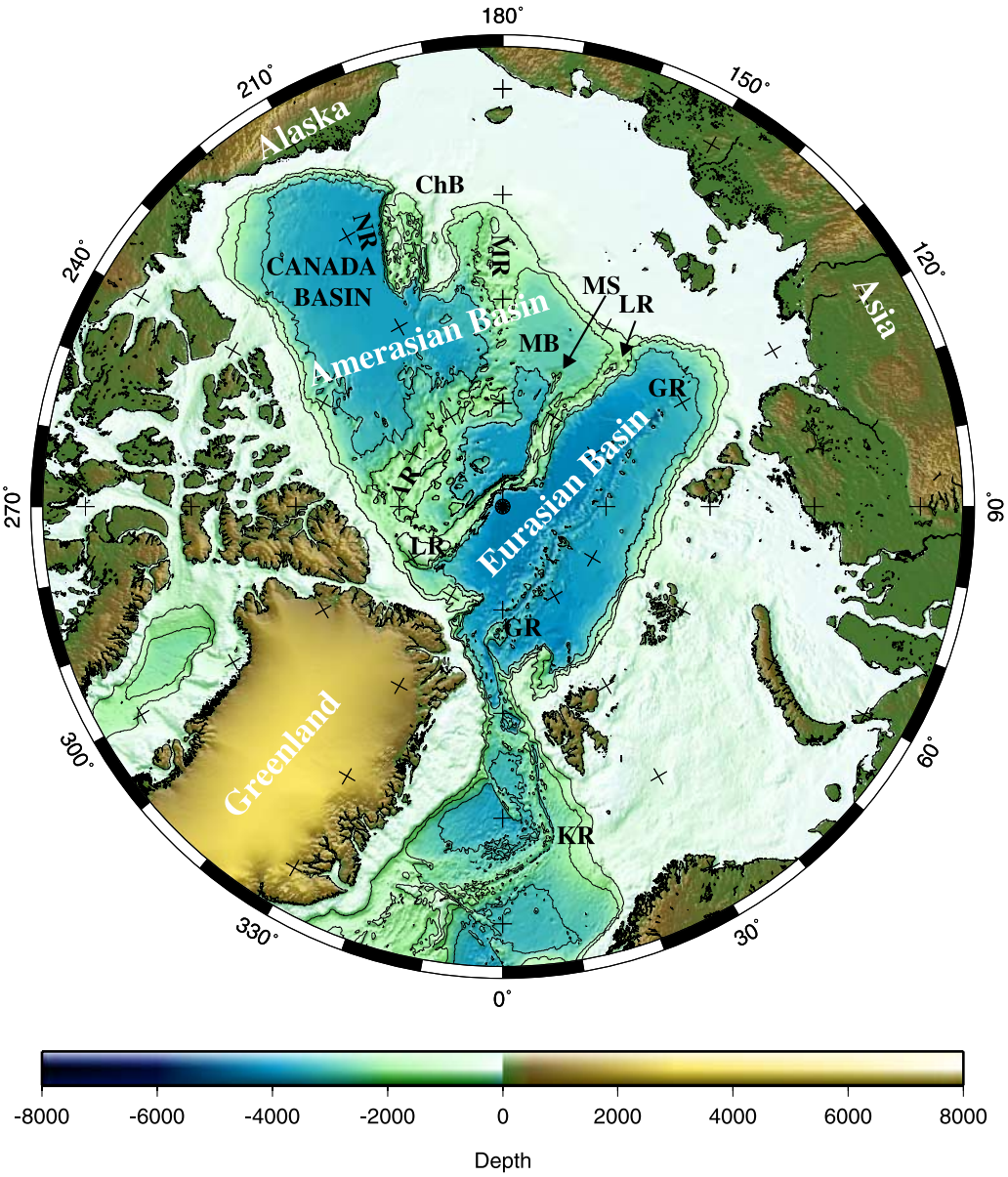

Figure 1. Arctic bathymetry and topography from IBCAO data grid [*Jakobsson et al.*, 2000]. Contours drawn at 1000, 2000, and 3000 m depths. Note large-scale physiographic features particularly the Eurasian Basin and the Amerasian Basin (AB), which are separated from each other by the Lomonosov Ridge (LR). Also note the Alpha Ridge (AR) and the Mendeleev Ridge (MR) in the AB as well as the Canada Basin which constitutes the southernmost AB plus the Makarov Basin (MB) which makes up the portion of the AB adjacent to the LR. The Marvin Spur (MS) lies in the southern Makarov Basin adjacent to the LR. The Chukchi Borderlands (ChB) are adjacent to the southwestern AB. The Gakkel Ridge (GR), which runs down the middle of the Eurasian Basin, is the site of active seafloor spreading and comprises the high-Arctic portion of the North American–Eurasian (NOAM-EUR) plate boundary. The NOAM-EUR plate boundary continues south from the GR though the Fram Strait (east of northernmost Greenland) to the Knipovich Ridge (KR) and thence along the rest of the northern half of the Mid-Atlantic Ridge.

the U.S. Navy with civilian collaborators made a series of six unclassified nuclear submarine cruises to the Arctic under the Science Ice Exercises (SCICEX) program [see, e.g., *Edwards and Coakley*, 2003; *Cochran et al.*, 2006; http://www.ldeo.columbia.edu/res/pi/SCICEX/]. Important new gravity and bathymetry over the Amerasian and Eurasian basins were collected on these SCICEX cruises. Starting in 1993, computation of detailed gravity in the ice-covered Arctic Ocean from the radar waveforms of the ERS-1 satellite altimeter [*Laxon and McAdoo*, 1994, 1998] became practical. These ERS-1 gravity fields revealed significant, previously uncharted, tectonic fabric in southern

Table 1. Five ICESat Campaigns Used

Laser Campaign	Start Date	End Date	Orbit Repeat, d	Data Release
1	20 Feb 2003	21 Mar 2003	8	18
2a	4 Oct 2003	18 Nov 2003	91/33	26
2b	19 Feb 2004	21 Mar 2004	91/33	26
3a	3 Oct 2004	8 Nov 2004	91/33	23
3b	17 Feb 2005	24 Mar 2005	91/33	19

portions (<81.5°N) of the AB, including for example, in the Canada basin, a gravity lineation associated with the presumed extinct axis of Mesozoic seafloor spreading [*Laxon and McAdoo*, 1994]. Despite all these new gravity and bathymetry data, the Amerasian Basin remains, for the most, a tectonic enigma. For an interesting account of the tectonic/geologic confusion, controversies, and potential international resource conflicts surrounding the Amerasian Basin and vicinity, see *Krajick* [2007]. The new ARCtic Satellite-only (ARCS) altimetric gravity field presented in this paper is shown to be valuable for testing and choosing among the various such tectonic models of the AB's origin and development. Also, the ARCS gravity field is important for the geodesist and gravity specialist. This paper demonstrates how the ARCS field complements, validates, and, in a number of places, improves upon the spatial resolution of state-of-the-art Arctic marine gravity fields (e.g., ArcGP) derived from surface observations.

2. Satellite Altimetric Gravity Over the Arctic Ocean

[4] In the 1990s, reprocessed return radar echoes from the ERS-1 satellite altimeter were used to compute detailed gravity fields for the ice-covered Arctic Ocean up to 81.5°N, ERS-1's northern limit of coverage [*Laxon and McAdoo*, 1994, 1998]. In this paper a much larger amount (8 years) of newly processed ERS-2 data is used to compute marine gravity. However, since ERS-2 occupies the same 98° inclination orbit as ERS-1, data coverage is limited to seas south of 81.5°N, and still leaves us with a 900-km radius polar hole in our altimetric gravity field of the Arctic Ocean. Fortunately laser altimetry from ICESat, launched in January 2003 [*Zwally et al.*, 2002; *Schutz et al.*, 2005], can be used to fill much of this polar hole and to map detailed gravity up to 86°N, ICESat's northern limit of coverage (ICESat occupies a more nearly polar, 94° inclination, orbit). Using a limited amount of early ICESat laser elevation data from the first two laser campaigns in 2003 and an "experimental lowest level filtering scheme," *Forsberg and Skourup* [2005, paragraph 8] demonstrated that a reasonable Arctic marine gravity field can be computed using ICESat data. In this paper we have combined five campaigns worth of ICESat data collected over a 2-year time span, and reduced via a newly developed waveform reprocessing scheme (see section 2.1), with the 8 years worth of ERS-2 data, to estimate the detailed ARCS marine gravity field exclusively from satellite data.

2.1. ICESat Laser Altimetry

[5] Although the primary mission of ICESat (launched January 2003) is to determine ice sheet elevation changes [*Schutz et al.*, 2005; *Zwally et al.*, 2002], return GLAS waveforms (or echoes) can also be used to estimate sea surface heights as well as sea ice freeboard in Arctic seas [*Farrell*, 2006a; *Kwok et al.*, 2004, 2006; *Zwally et al.*, 2003]. ICESat is composed of the spacecraft bus and the Geoscience Laser Altimeter System (GLAS). The GLAS makes the fundamental measurement, that of the range vector or the position of illuminated spot on the Earth's surface (e.g., the top of a sea ice floe or lead) with respect to the instrument. Complete details of how this measurement is made may be found in section 2 of *Schutz et al.* [2005]. GLAS laser footprints on the sea surface are typically 65–70 m in diameter and spaced ~170 m apart along track (40 Hz laser pulse frequency). As a consequence ICESat elevation profiles have potentially better along-track resolution than do ERS or Envisat altimeter profiles. ICESat elevations can have elevation accuracies of better than 3 cm. *Fricker et al.* [2005] demonstrated absolute elevation accuracy of corrected release 21 data for campaign L2a (see Table 1) approach 2 cm over salar de Uyuni, Bolivia. However, GLAS, unlike the ERS-2 altimeter, employs active pointing and so ICESat elevations are susceptible to systematic pointing (SPE) and geolocation errors [*Luthcke et al.*, 2005] which act as a source of elevation noise. These SPE can induce geographically correlated elevation errors on order several to 10 cm, but these can and have been reduced in recent rereleased (release > 19) data with error reduction-dependent upon specific campaign.

[6] The first estimates of Arctic sea ice freeboard were constructed [*Kwok et al.*, 2004] from along-track ICESat/GLAS data by using the elevation of open water to estimate the reference sea level. *Kwok et al.*'s [2004] technique for estimating sea level, which requires individual identification of recent openings via the use of complimentary RADARSAT imagery, is not suited for comprehensive, Arctic-wide mapping of sea surface topography. In our investigation, in order to compute gravity, we do a refined processing of ICESat waveform data to eliminate the sea ice freeboard signal (our 'noise') and thereby recover sea surface topography. We use techniques developed by *Farrell* [2006a], specifically the University College London (UCL) Algorithm, to distinguish ICESat waveforms reflected from mature sea ice, from those returned from leads or thin ice, and thereby retrieve sea surface heights (SSH) from ICESat/GLAS data over ice-covered seas. These SSH retrievals are, in turn, used to map mean sea surface (MSS) topography across the Arctic Ocean over a 2-year period.

[7] The key attribute of the UCL Algorithm is its ability to reliably discriminate and select GLAS echoes from leads using exclusively ICESat data and specific criteria related to elevation variation, reflectivity, and return pulse shape [*Farrell*, 2006a]. For example, a coincident drop in reflectivity and elevation can be indicative of thin ice in refrozen leads. The processing used in this investigation involves complex analyses of GLAS waveform characteristics in concert with GLAS elevations and reflectivity. While a full description of the processing approach is beyond the scope of this paper the reader is referred to *Farrell* [2006a] and *Farrell et al.* [2007] for further details. Similar techniques for the detection of leads and thin ice, as well as ICESat data characteristics over a variety of sea ice types, are described thoroughly by *Kwok et al.* [2006].

[8] Open, and recently refrozen, leads occupy only a small (1 to 5%) [*Wadhams*, 2000] portion of the central Arctic Ocean's winter pack ice but are widespread throughout the pack. In the application of the UCL Algorithm, the ICESat data are processed to effectively subselect data from leads alone and yield along-track sea surface height profiles wherein heights of mature ice, i.e., ice other than thin ice in leads, have been culled. Even though the lead fraction is small (<5%) at any given time, the overall lead detections in the ICESat data set we employed virtually blanket the Arctic Ocean (up to the northern limit of ICESat coverage, 86°N), owing partly to spatial redundancy afforded by five campaigns of ICESat data [*Farrell*, 2006a; *Farrell et al.*, 2006b; see also S. L. Farrell et al., manuscript in preparation, 2008]. The resulting individual sea surface height profiles are somewhat gap filled and noisy, but this is mitigated by implicit averaging of the ICESat data from frequent overlapping ground tracks. Nevertheless, effects of these gaps and noise may be evident in the ICESat gravity field derived below. In the near future, additional, and more highly refined, ICESat data will be used to further mitigate the effects of this noise. In this investigation, ICESat elevation data from five campaigns are used: GLAS Laser 1, 2a, 2b, 3a and 3b (see Table 1) which span from 20 February 2003 to 24 March 2005 [*Schutz et al.*, 2005]. All of the consequent derived profiles of along-track sea surface heights are then converted to along-track slopes (or deflection of vertical) for input into gravity anomaly computation (section 3).

2.2. ERS-2 Radar Altimetry

[9] ERS-2 was launched in April 1995 and occupies the same 98.5° inclination orbit as its predecessor, ERS-1. Eight years worth (84, 35-d cycles) of ERS-2 radar altimetry collected between May 1995 and June 2003 are used in this study. The techniques used for processing ERS-2 altimeter waveform data to extract precise sea surface heights over the ice-covered Arctic Ocean are essentially those described by *Peacock and Laxon* [2004] and *Laxon* [1994]. This waveform reprocessing substantially reduces the large sea surface height errors (of order several meters) produced over sea ice by the height tracking loops used onboard the ERS-2 altimeter. Accurate determination of the sea surface, as opposed to ice surface, elevations relies on reprocessing the specular waveform returns, which are the characteristic response of sea ice containing open or recently refrozen leads, to correct onboard height tracking errors. The large majority of ERS waveforms acquired over sea ice exhibit this specular response and can be reprocessed [*Peacock and Laxon*, 2004] to estimate sea surface elevation, thereby effectively eliminating contamination by sea ice freeboard "signals." (Related techniques to actually estimate the sea ice freeboard heights from ERS radar altimetry are developed by *Laxon et al.* [2003].) Derived profiles of along-track sea surface elevation are then converted to along-track slopes for input into gravity computations (section 3).

3. Gravity Field Computation

[10] Our approach relies on the fact that the mean sea surface (MSS) conforms, almost exactly, to a level surface, the geoid. In fact in the absence of wind, weather, tides and ocean dynamics, the MSS and geoid would be identical. After reprocessing both ICESat and ERS-2 altimetry waveforms using satellite-specific techniques described in sections 2.1 and 2.2, we are left with along-track profiles of sea surface topography which are accurate indicators of gravity anomalies particularly in the wavelength band of 25 to 600 km. We begin by constructing two separate Arctic marine fields: (1) an ICESat-only gravity field using just the ICESat along-track, sea surface slopes (see section 2.1) and relying on the methods of *McAdoo and Marks* [1992] [cf. *Laxon and McAdoo*, 1994, 1998; *Sandwell and Smith*, 1997] and (2) an ERS-2-only field using just the ERS-2 along-track slopes described in section 2.2 and relying on the same methods [*McAdoo and Marks*, 1992]. As the first, step 1, of our six steps, we preprocess and edit the ~10 Hz along-track sea surface heights to estimate and smooth [cf. *McAdoo and Marks*, 1992, p. 3252] the along-track slopes for both ICESat and ERS-2 data, using a Gaussian high-cut filter with a full width of 1.8 s (~12 km). This filtering suppresses high-frequency noise as well as signal at wavelengths less than 20 km, and also serves to edit outliers. Data gaps in individual passes do occur when fewer than five 10-Hz along-track points occur in a running 2-s window. However, because we average 84 35-d repeat cycles of ERS-2 data and five campaigns of ICESat data to form the four along-track slope grids (separate ascending and descending grids for both ERS-2 and ICESat; see step 2), this redundant spatial coverage fills nearly all data gaps. In step 2, we compute the four slope grids, before along-track slopes are low-cut filtered, by gridding with continuous curvature splines [*Wessel and Smith*, 1998] and by filling in the void over land with pseudoslopes computed by assuming that land gravity conforms exactly to the smoothed long-wavelength Gravity Recovery and Climate Experiment (GRACE) GGM02S geopotential [*Tapley et al.*, 2004] described in step 3. In other words, because our ARCS model is to be a satellite-only gravity field, no land gravimetry is used. Our gravity computation then proceeds (step 3) by low-cut filtering each of these four along-track slope grids by removing from these slopes a long-wavelength (>580 km) background geoid slope field, derived entirely from GRACE data. GRACE is a dedicated satellite gravity mission which, for the past 5 years, has been mapping the global geopotential with a spatial resolution of 400 to 40,000 km [*Tapley et al.*, 2004]. We derived the long-wavelength background gravity field by using a low-pass filtering of the GRACE-only GGM02S mean field [*Tapley et al.*, 2004; see also http://www.csr.utexas.edu/grace/gravity/] with a 580-km width Gaussian filter [see *McAdoo et al.*, 2005]. After the four grids of along-track slopes are low-cut filtered, we are left with band-limited along-track geoid slopes which can then, by flat Earth geodetic transformation, be transformed to band-limited gravity anomalies. Before this geodetic transformation can be performed, these along-track geoid slopes are converted (step 4) via vector algebra into true deflections of the vertical (north and east components) (see *McAdoo and Marks* [1992, equations (3a) and (3b)] or *Sandwell and Smith* [1997, Appendix B]). The resulting deflection-of-vertical (DOV) grids are Fourier transformed using conventional FFT techniques. Inverse Vening Meinesz transformation (step 5) of the DOV grids is accomplished [see *McAdoo*

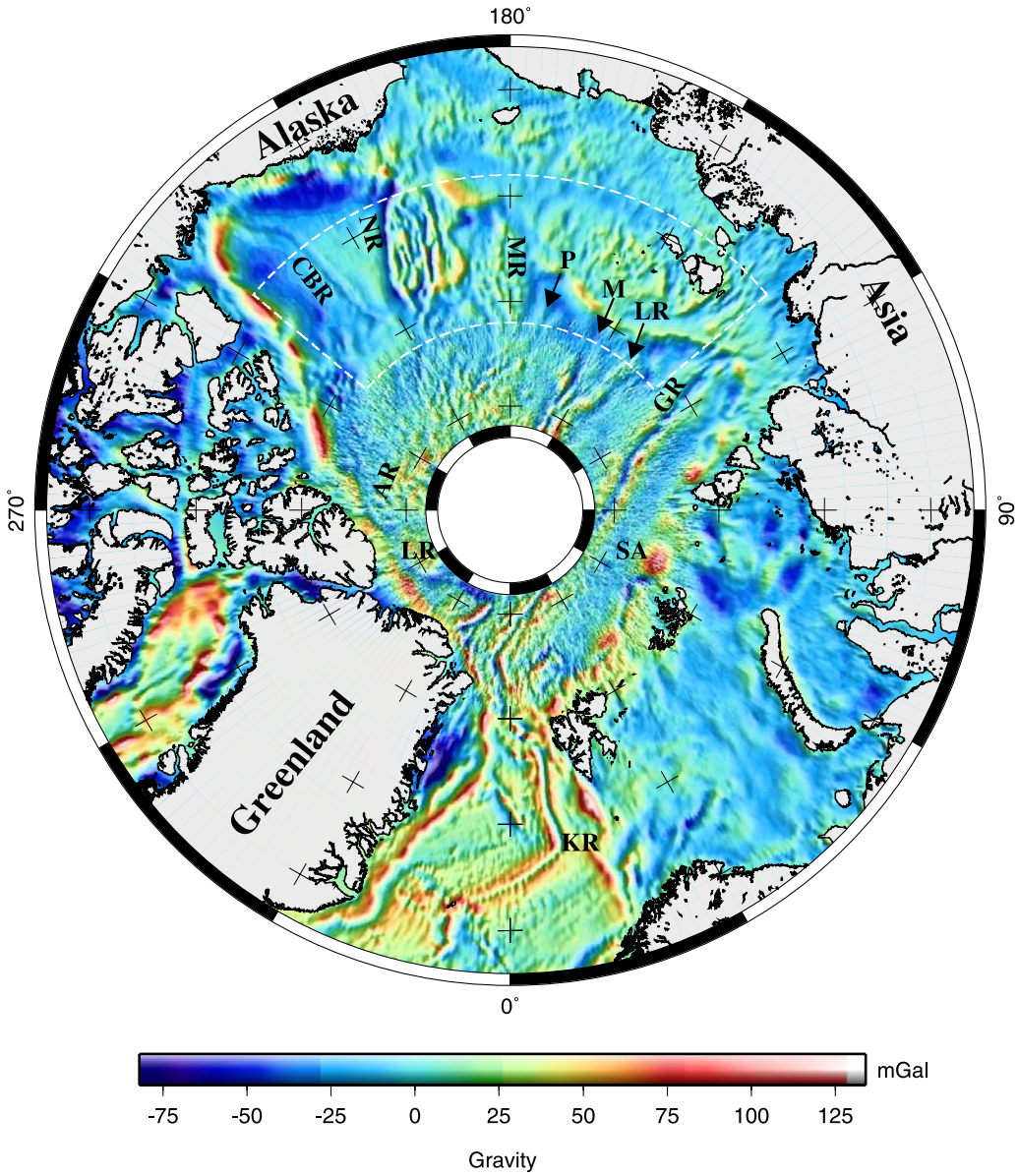

Figure 2. ARCtic Satellite-only (ARCS) marine gravity field computed using five campaigns worth of reprocessed ICESat/GLAS sea surface elevations and 8 years worth of ERS-2 retracked altimeter waveform data. Note gravitational expression of the Gakkel Ridge (GR), the KR, the LR, the MR, and the Northwind Ridge (NR) (see Figure 1 caption). Also note the north-south trending, lineated Canada Basin Ridge (CBR) gravity anomaly in the Canada Basin as well as the Podvodnikov (P) anomaly and the Marvin Spur extension (M) anomaly in the southern Makarov Basin plus the Saint Anna (SA) Trough gravity high (see text). Dashed white line encloses region F where gravity fields are intercompared (Figure 3). ARCS digital gravity is only displayed to 68°N but extends south to 60°N (see the auxiliary material).

and Marks, 1992, equation (A8); *Sandwell and Smith*, 1997; *Haxby et al.*, 1983] in the Fourier domain to finally yield, after inverse Fourier transformation, the band-limited gravity grids. Last (step 6), the long-wavelength GRACE GGM02S reference field is added back (restored) to the band-limited gravity to obtain (1) the final ICESat-only gravity field and (2) in a separate but parallel process, the final ERS-2-only gravity field. The ICESat-only and ERS-2-only gravity fields are then spliced, and in places blended, together to form the ARCS gravity field (Figure 2) which is registered on a 0.05° by 0.125° latitude-longitude output grid (see the auxiliary material[1]).The resulting ARCS field retains exclusively the ICESat-only gravity north of 81.5°N where there is no ERS data coverage. Also, south of 80.3°N, the ARCS field is taken entirely to be the ERS-2-only gravity field because the ERS-2-only field is based on many

[1]Auxiliary materials are available at ftp://ftp.agu.org/apend/jb/2007jb005217.

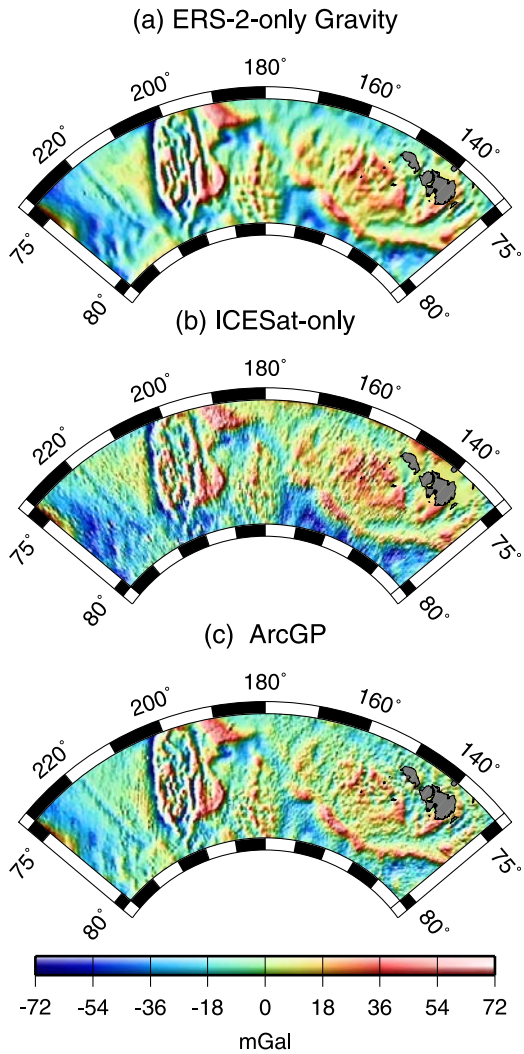

Figure 3. (a) ERS-2-only, (b) ICESat-only, and (c) ArcGP gravity field in region F (see Figure 2). For most of region F, the ERS-2-only gravity field is identical to the ARCS field (Figure 2). Note the similarity between all three fields and particularly the similarity between the ERS-2-only (Figure 3a), and the ArcGP field (Figure 3c). Each of the three fields is computed from entirely distinct data sets.

more data and is, as a result, more precise than the ICESat-only field (see, e.g., Figure 3 and related text in section 4.1). The ERS-2 data span 8 years and therefore can produce more of the beneficial temporal averaging than can the ICESat data. However, between 80.3°N and 81.5°N the ARCS gravity values are derived from a weighted mean of coincident ICESat and ERS-2 field values where weights are latitude-dependent and increasingly emphasize ICESat gravity at more northerly points.

4. Results

[11] The ARCS marine gravity field extends from 86°N to 60°N (compare auxiliary material) but is only displayed north of 68°N in Figure 2. Gravity anomalies which are clearly prominent in the ARCS field (Figure 2) include those associated with the bathymetrically prominent Gakkel Ridge (GR), the Knipovich Ridge (KR), the Lomonosov Ridge (LR), the Mendeleev (MR), the Northwind Ridge (NR), and the Chukchi Borderland (see Figure 1) as well as the generally positive anomalies which overlie the continental shelf edges that border the Eurasian and Amerasian basins. Note for example the belt of elongated positive gravity anomalies (Figure 2) flanking the eastern edge of the Amerasian Basin and running along the northwestern Canadian Arctic margin from the southeastern Beaufort Sea (near the MacKenzie Delta) to northernmost Ellesmere Island and the northern tip of Greenland. While gravity highs such as these are the norm along passive continental margins worldwide [e.g., *Watts and Stewart*, 1998] such gravity highs have been observed to be "particularly well developed" [e.g., *Vogt et al.*, 1998b, p. 459] along Arctic margins with amplitudes as large as 140 mGal or more. *Sobczak* [1975], *Vogt et al.* [1998a, 1998b], and others have also observed that these Arctic margin gravity highs (AMGHs) are located just landward of shelf breaks where Plio-Pleistocene glacial sediments have been deposited. *Sobczak* [1975] attributed some of these AMGHs to partially uncompensated, prograded wedges of Quaternary sediments. *Vogt et al.* [1998b, p. 473] suggested that these sediment depocenters alone may not fully account for the gravity high and that causally related, subjacent mass concentrations might have arisen beneath the depocenters due "perhaps" to "metastable (mineral) phase transitions" or other densification processes. However, Vogt et al.'s model of such high-density mass concentrations is controversial. A particularly large AMGH example, and one not identified by *Vogt et al.* [1998b], is the Saint Anna Trough gravity high just northeast of Franz Josef Land (see "SA" anomaly at 69°E, 82.5°N, Figure 2) which has an amplitude of ~145 mGal. Of even more tectonic interest, perhaps, than these gravity anomalies such as the GR, LR, NR, and KR, which have a clear, associated bathymetric expression, are those anomalies which have little or no bathymetric expression. For example, the Canada Basin portion of the Amerasian Basin displays a north-south trending lineated gravity low ("CBR" in Figure 2) but no corresponding bathymetric expression (Figure 1). The source of the CBR has been suggested [*Laxon and McAdoo*, 1994] (compare discussion by *Cochran et al.* [2006]) to be an extinct seafloor spreading ridge imprinted in the basement beneath a thick layer of sediments in support of rotational models for the opening of the Canada Basin. While the large sediment thicknesses of 6 to 10 km in the Canada Basin [*Grantz et al.*, 1990] are not typical of the entire Amerasian Basin (AB) other areas of the AB also have a rather thick sedimentary layer. One such area is the southern Makarov Basin, also known as the Podvonikov Basin (Figure 1), where sediment thicknesses approach 3.5 km [*Lebedeva-Ivanova et al.*, 2006] and where two north-south trending gravity lineations which we call the Podvodnikov and the Marvin Spur extension anomalies ("P" and "M" in Figure 2) are evident. Just as the CBR anomaly in the Canada Basin has no bathymetric expression, neither do the P and M anomalies (except the Marvin Spur proper which lies north of 83°N, see Figure 1). *Cochran et al.* [2006] observed this southerly extension of the Marvin Spur, or M anomaly, in SCICEX submarine gravity. *Cochran et al.*

Table 2. RMS Difference Between Gravity Fields in Region F[a]

Fields (Region F Only)	RMS Difference, mGal
ERS-2-only versus ArcGP gravity	6.96
ICESat-only versus ArcGP gravity	12.54
ICESat-only versus ERS-2-only	11.92

[a]See Figures 3a, 3b, and 3c.

[2006, p. 15] described it as part of the "outer ridge of the Lomonosov complex," and noted [p. 16] that it "continues south along 157°E to the Siberian margin" as can be seen in Figure 2. Both the P and the (southern) M anomaly are most likely due to ridge-like basement topography imprinted in the basement and masked by overlying sediments. Possible tectonic significance of these anomalies is discussed in section 5.

4.1. Accuracy and Resolution

[12] To assess the accuracy and spatial resolution of the ARCS field we intercompare the ERS-2-only field (Figure 3a) with the ICESat-only field (Figure 3b) and the ArcGP gravity field (Figure 3c) in the region F. Region F was chosen because it is a large portion of the ice-covered Arctic Ocean which has both complete ERS-2 and ICESat coverage. Therefore, in region F, three gravity fields computed from three independent data sets can be compared. While good agreement is evident between all three fields, the ERS-2-only field (Figure 3a) appears to display gravity details most clearly, and with the least noise, of the three. Again note that while the overall ARCS field is a combination of ERS-2-only and ICESat-only fields, south of 80.3°N it is composed exclusively of ERS-2-only gravity. The ICESat-only field is plainly noisier than the ERS-2 field as a result of being computed from a much smaller data set than the ERS-2 field. The ArcGP field is constructed largely using surface (as opposed to satellite) gravity with the notable exception of part of the Siberian continental shelf area (130°E to 180°E, the right half of region F, Figure 3c) where raw surface gravity data were not available and ERS-1 gravity from *Laxon and McAdoo* [1998] were used instead [*Forsberg and Kenyon*, 2004]. The ArcGP data agrees well with the ERS-2 field. In the left half of region F (180°E to 230°E), ArcGP is almost exclusively computed from a densely spaced set of accurate Naval Research Laboratory (NRL) airborne gravimetric surveys [cf. *Childers et al.*, 2001, Figure 2] which blanket this region, and the ArcGP is therefore arguably more accurate in region F (left half) than most, if not all, other regions of the high Arctic. Over the entire region F, the RMS difference between the ERS-2-only field (Figure 3a) and the ArcGP gravity (Figure 3c) is 6.96 mGal (Table 2). The corresponding RMS difference in region F between the ERS-1 and ArcGP gravity is 5.73 mGal. So recalling that the ArcGP is identical to the ERS-1 field for the right half (130°E to 180°E) of region F, it is remarkable that the ERS-2 – ArcGP RMS difference of 6.96 mGal is just 1.2 mGal more than the ERS-1 – ArcGP difference. Furthermore, that the new ERS-2 field (unlike the ERS-1 field which did employ surface gravity over land) uses satellite data only and does not include any surface gravity data, underscores the significance of the low ERS-2 – ArcGP difference of 6.96 mGal. The RMS difference between the ERS-2-only (Figure 3a) and the ICESat-only gravity (Figure 3b) in region F is 11.92 mGal (Table 1). The larger RMS difference results from the noisier ICESat-only field (Figure 3b). Of course in most of region F (i.e., south of 80.3°N) our final ARCS field employs exclusively the more precise ERS-2-only gravity and only employs the ICESat gravity north of 80.3°N. Cross-spectral analysis of the ERS-2-only field and the ArcGP field yields coherences (Figure 4) between the two fields of greater than 0.5 at all wavelengths > 35 km. Therefore both the ERS-2 and ArcGP fields confidently resolve gravity to wavelengths as short as 35km. Coherences between the ERS-2 and ICESat-only fields (Figure 4) are generally somewhat less than between ERS-2 and ArcGP. They drop to 0.5 at a 50 km wavelength due to the ICESat-only field being slightly noisier and therefore resolving gravity only to wavelengths as short as 50 km. Note, however, that at wavelengths longer than 380 km, the ERS-2 versus ICESat coherences are very slightly higher than the ERS-2 versus ArcGP coherences, as opposed to less at wavelengths shorter than 250 km. Since both ERS-2 and ICESat fields used GRACE GGM02S gravity at long wavelengths these slightly higher coherences might reflect the enhanced long-wavelength accuracy of GRACE GGGMO2S.

4.2. Comparison With Submarine and Airborne Gravity

[13] North of 81.5°N, the northern limit of ERS-2 coverage, intercomparison of ERS-2 and ICESat gravity is not possible. At these high latitudes, the ARCS gravity field is computed entirely from ICESat data and we validate the ARCS field here using submarine gravity data (Figure 5a) such as that collected by the 1993 SCICEX cruise of the U.S. Navy nuclear submarine, Pargo [*Cochran et al.*, 2003; *Edwards and Coakley*, 2003]. In Figure 5a, both the Pargo submarine gravity profile (blue) and the coincident satellite

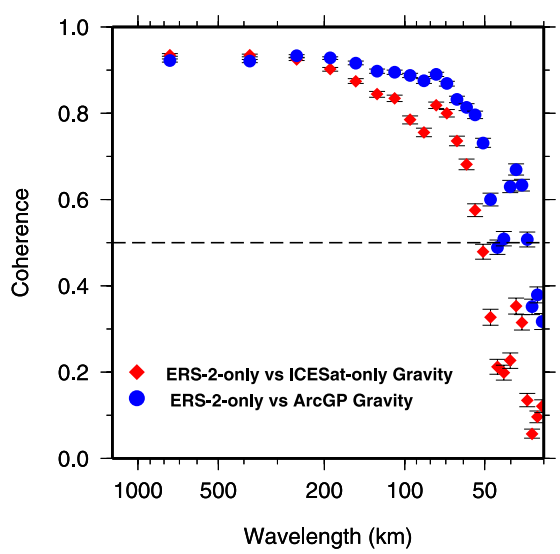

Figure 4. Spectral coherency (east-west component) in region F: (1) between ERS-2-only and ICESat-only field (red diamonds); and (2) between ERS-2-only and ArcGP (blue circles).

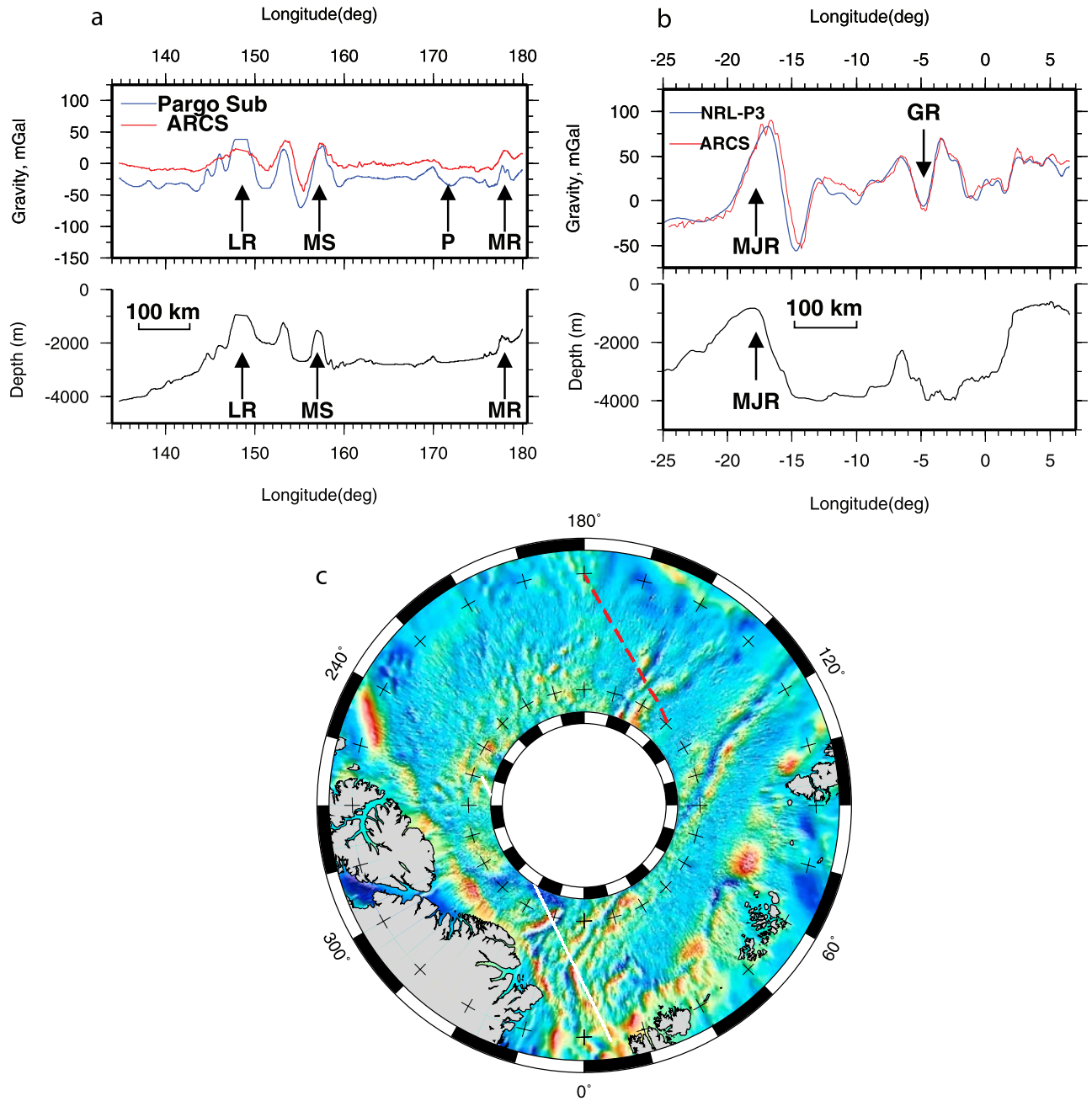

Figure 5. (a) Free-water submarine gravity (blue) from 1993 SCICEX cruise of USN Pargo and ARCS satellite gravity (red) interpolated onto Pargo track (shown in dashed red in Figure 5c). Bathymetry (black) is interpolated from IBCAO grid. Note the Lomonosov Ridge (LR), Marvin Spur (MS), and Mendeleev Ridge (MR) expressed in the bathymetry and gravity and Podvodnikov (P) anomaly in the gravity. (b) An airborne free-air gravity profile (blue) from the 1998 NRL P-3 Arctic survey and ARCS satellite gravity (red) interpolated onto P-3 track (shown in white in Figure 3c). Bathymetry (black) is interpolated from IBCAO grid. Note the axial gravity low over the Gakkel Ridge (GR) and the large anomaly associated with the Morris Jessup Rise (MJR) are well expressed in both NRL airborne and ARCS satellite gravity. (c) Map of area discussed in Figures 5a and 5b.

gravity profile (red), interpolated from the ARCS grid, display anomalies whose sources are the Lomonosov Ridge (LR), Marvin Spur (MS), and Mendeleev Ridge (MR). Moreover both the submarine and the ARCS gravity profiles reveal the Podvodnikov anomaly (P) (compare Figure 2). This profile comparison (Figure 5a) indicates that both the submarine and the ARCS gravity clearly resolve features of 50 km wavelength (e.g., MR in Figure 5a) and longer. However, the SCICEX submarine gravity has a decidedly and understandably better resolving capability than the ARCS gravity. In the limited areas where they are available, the SCICEX data undoubtedly do a better job of resolving

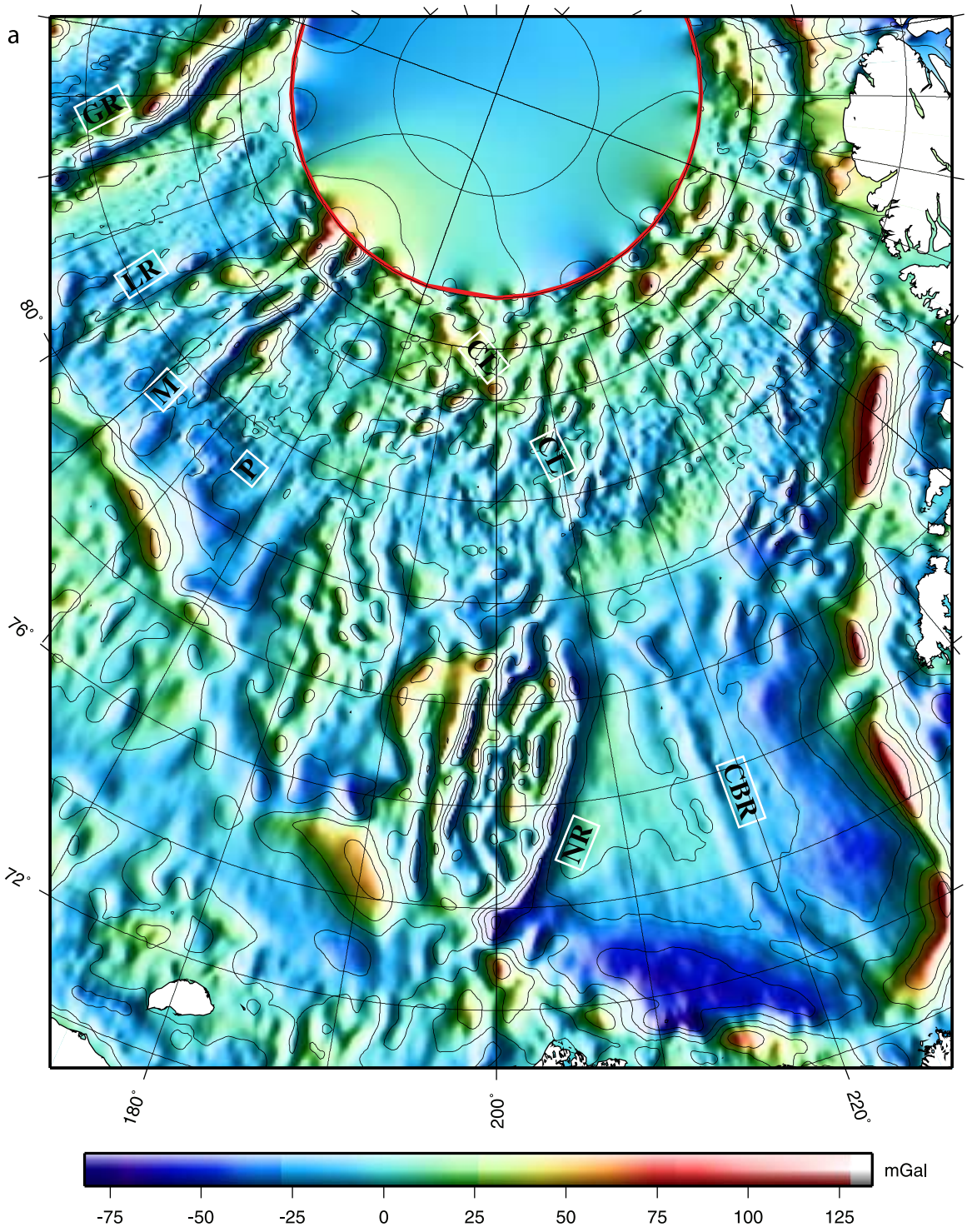

Figure 6. (a) ARCS satellite marine gravity field. ARCS gravity is the same as that in Figure 2 but reprojected and zoomed in on, exclusively, the Amerasian Basin. Note labeling of the Canada Basin Ridge (CBR) anomaly, the Podvodnikov (P) anomaly, the Marvin Spur extension (M) anomaly, the Northwind Ridge (NR), the Charlie Lineation (CL), Lomonosov Ridge (LR) and Gakkel Ridge (GR). Northern limit of ICESat coverage, 86°N, is drawn in red (both panels). (b) The Chukchi Borderland (ChB) is labeled, and 1000, 2000, and 3000 m depth contours are drawn in black.

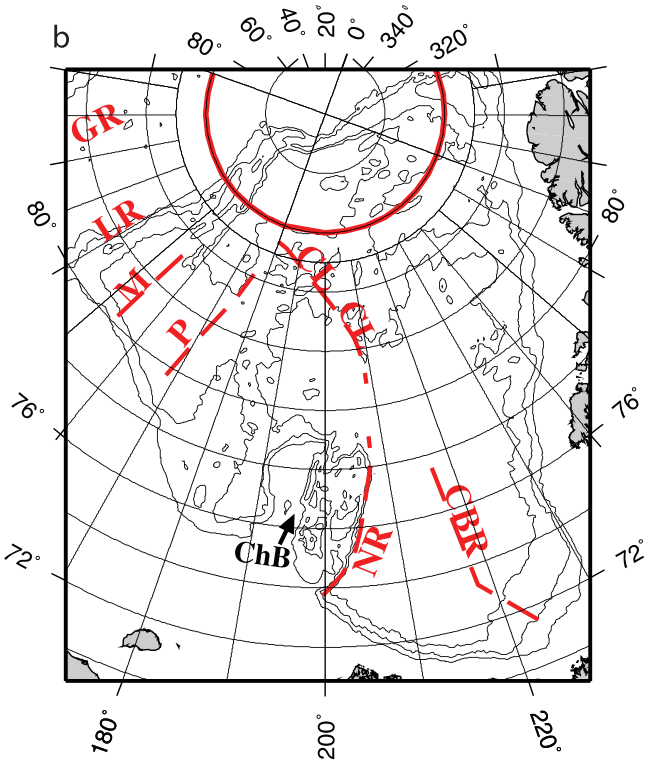

Figure 6. (continued)

fine-scale gravity (e.g., 20-km wavelengths) than any of the other observing techniques employed in the Arctic Ocean [cf. *Edwards and Coakley*, 2003; *Childers et al.*, 2001]. There is an obvious offset, or bias, between the two gravity profiles in Figure 5a: the submarine gravity is, in the mean, 23 mGal less than the ARCS satellite gravity. Most likely it is the Pargo submarine gravity data which are biased low here as they have not been subjected to a formal cross over analysis with respect to other survey tracks (J. R. Cochran, personal communication, 2005). In Figure 5b, an airborne gravity profile (blue) from a 1998 NRL Arctic survey [*Childers et al.*, 2001] and the coincident satellite gravity profile (red), interpolated from the ARCS grid, agree closely with each other. The agreement between the two gravity profiles is very good with a mean and RMS difference of 2.6 and 7.8 mGal respectively. Furthermore one can see in both gravity profiles (Figure 5b) a ~50 mGal axial gravity low over the actively, but slowly spreading Gakkel Ridge (GR), and a ~120 mGal anomaly associated with the Morris Jessup Rise (MJR).

5. Discussion

[14] This detailed ARCS marine gravity field (see Figure 2; also auxiliary material) reveals the rich tectonic fabric of the Arctic Basin up to the northern limit of ICESat coverage (86°N). The comparisons described in section 4.1 show that the southern (<80.3°N) ARCS gravity field (based on ERS-2) has an amplitude precision of ~6 mGal or better and a spatial resolution as fine as ~35 km. The northern part of ARCS gravity field (based on ICESat data) is only slightly inferior in resolution of detail and precision to the southern ARCS and can resolve gravity to wavelengths as short as 50 km. The ARCS gravity field is a satellite-only field, but it agrees closely, over much of the Arctic Ocean, with the fully independent surface gravity field, ArcGP, while in places revealing more detail than the ArcGP.

[15] Three important new tectonic details in the central Arctic portion of the ARCS field were discussed in section 4. These are the Canada Basin Ridge (CBR), the Podvodnikov (P) anomaly, and the M anomaly which is associated with the "outer ridge" or southerly extension of the Marvin Spur. These three are all located in the Amerasian Basin (AB; Figure 6) and are all (bathymetrically) hidden between thick sediments that tend to cover most of the AB. Presumably all three anomalies have, as their source, topography imprinted in the basement beneath layers of sediments. For example the Canada Basin Ridge (CBR; Figure 6) anomaly has been proposed [*Laxon and McAdoo*, 1994, 1998] to be an extinct seafloor spreading ridge imprinted in the basement topography. This putative CBR spreading center supports the widely held, but still controversial [cf. *Cochran et al.*, 2006; *Lawver and Scotese*, 1990], hypothesis that much of the triangular Amerasian Basin (Figure 6) formed in Cretaceous time by rifting, subsequent seafloor spreading, and consequent counterclockwise rotational motion of a large crustal block away from that which is now the western edge of the Canadian Archipelago [*Lawver and Scotese*, 1990]. This rotation was proposed to have taken place around a kinematic pole lying in the MacKenzie Delta area of northwestern Canada [see, e.g., *Grantz et al.*, 1998]. The *1992 Arctic Summer West Scientific Party* [1993] have pointed out, however, that the Chukchi Borderland (see ChB, Figures 1 and 6) presents "a space problem" for this rotational opening hypothesis for the Amerasian/Canada Basin; i.e., the Chukchi Borderland (ChB) gets in the way. The *1992 Arctic Summer West Scientific Party* [1993] and *Grantz et al.* [1998] propose instead that the Northwind Ridge (NR) is a continental fragment which broke away from adjacent continents around 90 Ma and that the NR as well, presumably, as attached portions of the ChB, were transported into the Amerasian Basin in Tertiary time, i.e., after the opening of the Canada Basin which occurred earlier (at approximately 125 Ma). They also suggested this transporting process was associated with east-west extension within basins or crustal blocks of the ChB and was accommodated in part by motion along a postulated "Charlie transform fault" which might trace west from the northern end of the Northwind Ridge (NR) to the Eurasian Basin [see, e.g., *Grantz et al.*, 1998, Figures 1 and 7]. In Figure 6 a gravity lineation which we shall call the Charlie lineation (CL) can be traced from the northern end of the NR in an arc trending northwest and then west across the Mendeleev Ridge and the Makarov Basin to an intersection with the Lomonosov Ridge at ~160°E, 86°N. This Charlie lineation (CL) follows roughly but not exactly the proposed trace of the Charlie transform fault hypothesized by *1992 Arctic Summer West Scientific Party* [1993] and *Grantz et al.* [1998], and we suggest that it might be evidence of such proposed transform motion. Moreover we speculate that the Podvonikov (P) anomaly (Figures 2 and 6) in the Makarov Basin might be the locus of an extinct spreading ridge(s) along with the CBR

anomaly in the Canada Basin. We note, however, that our suggestion the P anomaly could be the trace of an extinct spreading ridge is not consistent with the proposition of possible east-west trending, seafloor spreading magnetic anomalies [*Glebovsky et al.*, 2000; L. C. Kovacs, personal communication, 2002]. Extension along an extinct axis such as that represented by the P anomaly might be related to transport (in the early Tertiary) of continental fragments including the Northwind Ridge. But these are just tectonic clues, inasmuch as gravity fields alone can only provide indications of tectonic motions, and owing to gravity's nonuniqueness, one requires corroborative data such as seismics in order to make totally definitive statements about the source of these anomalies and related tectonic deformation. We should also note, however, that *Cochran et al.* [2006] suggest the Marvin Spur is a continental sliver from the Lomonosov Ridge block and may be the trace of a transform boundary which accommodated a rotational opening of the entire AB. Also a reflection seismic line transecting the P anomaly (see the Arctic 2000 line and Figure 10 of *Lebedeva-Ivanova et al.* [2006]) appears to be consistent with the hypothesis that the P anomaly may be an extinct spreading center buried by overlying sediments. Much research remains to solve the mystery of the Amerasian Basin's tectonic history; this gravity field will provide only a limited set of constraints and clues which should help unravel the history. The AB is indeed an "enigmatic. . .deep hole" (section 1.1) and surely more enigmatic than any of the world's small-to-medium ocean basins.

6. Summary

[16] The ARCS gravity field presented and tested in this paper is a detailed, satellite-only Arctic marine field which generally corroborates, and often improves upon, the fully independent Arctic gravity field, ArcGP, which was derived from surface observations [*Forsberg and Kenyon*, 2004]. The new ARCS field provides uniformly dense coverage of all Arctic seas south of 86°N and reveals more detail than the ArcGP in many places where ArcGP data coverage is sparse. In most areas ARCS confidently resolves gravity anomalies with wavelengths as short as 35 km. The ARCS field will prove valuable for constraining tectonic models of the Arctic Ocean Basin's development particularly for resolving the tectonic enigma which the Amerasian Basin (AB) represents. ARCS reveals gravity lineations and tectonic fabric (e.g., the Podvodnikov anomaly, the Canada Basin Ridge, and the Marvin Spur extension anomaly), which are clues to the AB's tectonic history. Future improved versions of the ARCS field will include many more ICESat data which should enhance precision as well as resolution, and ultimately, CryoSat2 data, which will extend coverage north from 86°N to 88°N.

[17] **Acknowledgments.** We gratefully acknowledge NASA's ICESat Science Project and the NSIDC for distribution of the ICESat data; see http://icesat.gsfc.nasa.gov and http://nsidc.org/data/icesat/. We thank Vicki Childers and John Brozena of the Naval Research Laboratory (NRL) for helpful advice and providing a line of NRL airborne gravity data. We also thank Jim Cochran (Lamont-Doherty Earth Observatory) for providing and helping with SCICEX gravity data. The late William F. (Bill) Haxby is gratefully acknowledged for his pioneering work in mapping marine gravity with satellite altimeter data. We thank Arthur Grantz and two anonymous referees for their most helpful reviews. Contents of this manuscript are solely the opinions of the authors (D.C.M.) and do not constitute a statement of policy, decision, or position on behalf of NOAA.

References

1992 Arctic Summer West Scientific Party (1993), Cruise to the Chukchi borderland, Arctic ocean, *Eos Trans. AGU*, *74*(22), 249.

Childers, V. A., D. C. McAdoo, J. M. Brozena, and S. W. Laxon (2001), New gravity data in the Arctic Ocean: Comparison of airborne and ERS gravity, *J. Geophys. Res.*, *106*(B5), 8871–8886, doi:10.1029/2000JB900405.

Cochran, J. R., G. J. Kurras, M. H. Edwards, and B. J. Coakley (2003), The Gakkel Ridge: Bathymetry, gravity anomalies, and crustal accretion at extremely slow spreading rates, *J. Geophys. Res.*, *108*(B2), 2116, doi:10.1029/2002JB001830.

Cochran, J. R., M. H. Edwards, and B. J. Coakley (2006), Morphology and structure of the Lomonosov Ridge, Arctic Ocean, *Geochem. Geophys. Geosyst.*, *7*, Q05019, doi:10.1029/2005GC001114.

Edwards, M. H., and B. J. Coakley (2003), SCICEX Investigations of the Arctic Ocean System, *Chem. Erde*, *63*, 281–328, doi:10.1078/0009-2819-00039.

Farrell, S. L. (2006), Satellite laser altimetry over sea ice, Ph.D. dissertation, Univ. College London, London.

Farrell, S. L., D. C. McAdoo, S. W. Laxon, H. J. Zwally, D. Yi, and A. L. Ridout (2006), A new arctic marine gravity field derived using ICESat altimetry: Tectonic implications, *Eos Trans. AGU*, *87*(52), Fall Meet. Suppl., Abstract T53B–1597.

Farrell, S. L., S. W. Laxon, A. L. Ridout, and D. C. McAdoo (2007), Combining ICESat and ENVISAT altimetry over sea ice, paper presented at IUGG XXIV General Assembly, Int. Union of Geod. and Geophys., Perugia, Italy, 2–13 July.

Forsberg, R., and S. Kenyon (2004), Gravity and geoid in the Arctic region—The northern polar gap now filled, paper presented at ESA GOCE User Workshop, Eur. Space Agency, Frascati, Italy.

Forsberg, R., and H. Skourup (2005), Arctic Ocean gravity, geoid and sea-ice freeboard from ICESat and GRACE, *Geophys. Res. Lett.*, *32*, L21502, doi:10.1029/2005GL023711.

Fricker, H. A., A. Borsa, B. Minster, C. Carabajal, K. Quinn, and B. Bills (2005), Assessment of ICESat performance at the salar de Uyuni, Bolivia, *Geophys. Res. Lett.*, *32*, L21S06, doi:10.1029/2005GL023423.

Glebovsky, V. Y., L. C. Kovacs, S. P. Maschenkov, and J. M. Brozena (2000), Joint compilation of Russian and US Navy aeromagnetic data in the central Arctic seas, *Polarforschung*, *68*, 35–40.

Grantz, A., S. D. May, P. T. Taylor, and L. Lawver (1990), Canada Basin, in *The Geology of North America*, vol. L, *The Arctic Ocean Region*, edited by A. Grantz, G. L. Johnson, and J. F. Sweeney, pp. 379–401, Geol. Soc. of Am., Boulder, Colo.

Grantz, A., D. L. Clark, R. L. Phillips, and S. P. Srivastava (1998), Phanerozoic stratigraphy of Northwind Ridge, magnetic anomalies in the Canada Basin, and the geometry and timing of rifting in the Amerasian Basin, Arctic Ocean, *Geol. Soc. Am. Bull.*, *110*, 801–820, doi:10.1130/0016-7606(1998)110<0801:PSONRM>2.3.CO;2.

Haxby, W. F., G. D. Karner, J. L. LaBrecque, and J. K. Weissel (1983), Digital images of combined oceanic and continental data sets and their use in tectonic studies, *Eos Trans. AGU*, *64*(52), 995–1004.

Jakobsson, M., N. Cherkis, J. Woodward, R. McNab, and B. Coakley (2000), New grid of Arctic bathymetry aids scientists and mapmakers, *Eos Trans. AGU*, *81*, 89–96, doi:10.1029/00EO00059.

Krajick, K. (2007), News: Race to plumb the frigid depths, *Science*, *315*(5818), 1525–1528, doi:10.1126/science.315.5818.1525.

Kwok, R., H. J. Zwally, and D. Yi (2004), ICESat observations of Arctic sea ice: A first look, *Geophys. Res. Lett.*, *31*, L16401, doi:10.1029/2004GL020309.

Kwok, R., G. F. Cunningham, H. J. Zwally, and D. Yi (2006), ICESat over Arctic sea ice: Interpretation of altimetric and reflectivity profiles, *J. Geophys. Res.*, *111*, C06006, doi:10.1029/2005JC003175.

Lawver, L. A., and C. R. Scotese (1990), A review of tectonic models for the evolution of the Canada Basin, in *The Geology of North America*, vol. L, *The Arctic Ocean Region*, edited by A. Grantz, G. L. Johnson, and J. F. Sweeney, pp. 593–618, Geol. Soc. of Am., Boulder, Colo.

Laxon, S. (1994), Sea ice altimeter processing scheme at the EODC, *Int. J. Remote Sens.*, *15*, 915–924.

Laxon, S. W., and D. C. McAdoo (1994), Arctic Ocean gravity field derived from ERS-1 satellite altimetry, *Science*, *265*, 621–624, doi:10.1126/science.265.5172.621.

Laxon, S., and D. McAdoo (1998), Satellites provide new insights into polar geophysics, *Eos Trans. AGU*, *79*(6), 69, doi:10.1029/98EO00045.

Laxon, S. W., N. Peacock, and D. Smith (2003), High interannual variability of sea ice in the Arctic region, *Nature*, *425*, 947–950, doi:10.1038/nature02050.

Lebedeva-Ivanova, N. N., Y. Y. Zamansky, A. E. Langinen, and M. Y. Sorokhin (2006), Seismic profiling across the Mendeleev Ridge of 82°N: Evidence of continental crust, *Geophys. J. Int.*, *165*, 527–544, doi:10.1111/j.1365-246X.2006.02859.x.

Luthcke, S. B., D. D. Rowlands, T. A. Williams, and M. Sirota (2005), Reduction of ICESat systematic geolocation errors and the impact on ice sheet elevation change detection, *Geophys. Res. Lett.*, *32*, L21S05, doi:10.1029/2005GL023689.

McAdoo, D. C., and K. M. Marks (1992), Gravity fields of the Southern Ocean from Geosat data, *J. Geophys. Res.*, *97*(B3), 3247–3260, (Correction to "Gravity fields of the Southern Ocean from Geosat data," *J. Geophys. Res.*, *97*(B12), 17,709, 1992.)

McAdoo, D., C. Wagner, and S. W. Laxon (2005), Improvements in Arctic gravity and geoid from CHAMP and GRACE: An evaluation, in *Earth Observation With CHAMP: Results From Three Years in Orbit*, edited by C. Reigber et al., pp. 37–46, Springer, Berlin.

Ostenso, N. A., and R. J. Wold (1973), Aeromagnetic evidence for origin of Arctic Ocean Basin, in *Arctic Geology*, edited by M. G. Pitcher, pp. 506–516, Am. Assoc. of Pet. Geol, Tulsa, Okla.

Peacock, N. R., and S. W. Laxon (2004), Sea surface height determination in the Arctic Ocean from ERS altimetry, *J. Geophys. Res.*, *109*, C07001, doi:10.1029/2001JC001026.

Sandwell, D. T., and W. H. F. Smith (1997), Marine gravity anomaly from Geosat and ERS-1 satellite altimetry, *J. Geophys. Res.*, *102*(B5), 10,039–10,054, doi:10.1029/96JB03223.

Schutz, B. E., H. J. Zwally, C. A. Shuman, D. Hancock, and J. P. DiMarzio (2005), Overview of the ICESat Mission, *Geophys. Res. Lett.*, *32*, L21S01, doi:10.1029/2005GL024009.

Sobczak, L. W. (1975), Gravity and deep structure of the continental margin of Banks Island and MacKenzie Delta, *Can. J. Earth Sci.*, *12*, 378–394.

Tapley, B. D., S. Bettadpur, M. Watkins, and C. Reigber (2004), The gravity recovery and climate experiment: Mission overview, *Geophys. Res. Lett.*, *31*, L09607, doi:10.1029/2004GL019920.

Taylor, P. T., L. C. Kovacs, P. R. Vogt, and G. L. Johnson (1981), Detailed aeromagnetic investigations of the Arctic Basin: 2, *J. Geophys. Res.*, *86*(B7), 6323–6330, doi:10.1029/JB086iB07p06323.

Tessensohn, F., and N. W. Roland (2000), ICAM III: Third International Conference on Arctic Margins, *Polarforshung*, *68*, 1–9.

Vogt, P., W. Y. Jung, and J. Brozena (1998a), Arctic margin gravity highs remain puzzling, *Eos Trans. AGU*, *79*(49), 601, doi:10.1029/98EO00433.

Vogt, P. R., W. Y. Jung, and J. M. Brozena (1998b), Arctic margin gravity highs: Deeper meaning for sediment depocenters?, *Mar. Geophys. Res.*, *20*, 459–477, doi:10.1023/A:1004775228851.

Wadhams, P. (2000), *Ice in the Ocean*, 351 pp., Gordon and Breach, Amsterdam, Netherlands.

Watts, A. B., and J. Stewart (1998), Gravity anomalies and segmentation of the continental margin offshore West Africa, *Earth Planet Sci. Lett.*, *156*, 239–252, doi:10.1016/S0012-821X(98)00018-1.

Wessel, P., and W. H. F. Smith (1998), New, improved version of generic mapping tools released, *Eos Trans. AGU*, *79*(47), 579, doi:10.1029/98EO00426.

Zwally, H. J., et al. (2002), ICESat's laser measurements of polar ice, ocean, atmosphere and land, *J. Geod.*, *34*, 405–445, doi:10.1016/S0264-3707(02)00042-X.

Zwally, H. J., A. C. Brenner, S. L. Farrell, S. W. Laxon, and D. Yi (2003), Deriving sea-ice freeboard height distributions and estimates of ice thickness from ICESat/GLAS laser altimetry, *Eos Trans. AGU*, *84*(46), Fall Meet. Suppl., Abstract C32A–0442.

S. L. Farrell, S. W. Laxon, and A. L. Ridout, Centre for Polar Observation and Modelling, University College London, Gower Street, London, WC1E 6BT, UK. (slf@cpom.ucl.ac.uk; swl@cpom.ucl.ac.uk; alr@cpom.ucl.ac.uk)

D. C. McAdoo, NOAA Laboratory for Satellite Altimetry, 1335 East-West Highway, Silver Spring, MD 20910-3282, USA. (dave.mcadoo@noaa.gov)

D. Yi, SGT, Inc., NASA Goddard Space Flight Center, Greenbelt, MD 20771, USA. (doughui@icesat2.gsfc.nasa.gov)

H. J. Zwally, Cryospheric Sciences Branch, Code 614.1, NASA Goddard Space Flight Center, Greenbelt, MD 20771, USA. (zwally@icesat2.gsfc.nasa.gov)